Solid State Phenomena
ISSN: 1662-9779, Vol. 387, pp 21-31
doi:10.4028/p-91sVZi

Submitted: 2025-12-19
Revised: 2026-02-14
Accepted: 2026-02-14
Online: 2026-04-14

Stability of Tubular Preforms from Multi-Layer Winding of Composite Tapes Prior to Thermoforming

Nagui ELGABY[1,2,a*], Guillaume HELBERT[1,b] , Nahiene HAMILA[1,c]
Ruben CAMPOS[2,d], Audrey SANCHEZ[2,e] , Bertrand LAINE[2,f]

[1]CNRS, IRDL UMR 6027, Bretagne INP, Plouzané, 29280, France

[2]OLLOW, 7 Avenue de Guitayne, 33610 Canéjan, France

[a]nagui.elgaby@enib.fr, [b]guillaume.helbert@enib.fr, [c]nahiene.hamila@enib.fr
[d]rcampos@ollow-tech.com, [e]asanchez@ollow-tech.com, [f]blaine@ollow-tech.com

Keywords: Tape winding, Stability, Tubular composites

Abstract. Some composite preforms lose dimensional stability after mandrel removal during tube winding, leading to pronounced longitudinal expansion and radial contraction for specific layup configurations. This work presents an experimental method for tracking the reorganization of individual wound tapes during mandrel release and uses these measurements to validate a finite element (FE) model designed to capture the underlying deformation mechanisms. The experiments reveal a nonlinear dependence of ribbon elongation on the initial winding angle. Complementary FE parametric studies investigate the effects of tape geometry and mechanical properties, demonstrating that increased mechanical anisotropy amplifies the elongation response. The study also introduces a layer-equivalent stiffness formulation and concludes with FE simulations of multi-tape preforms. Together, these results support the development of improved winding strategies aimed at reducing defects, lowering production costs, and enhancing the structural performance of tubular composite components.

Introduction

Tubular composite structures are increasingly utilized across sectors such as oil and gas, civil engineering, automotive, and aerospace, owing to their high specific strength and stiffness, which make them well suited for lightweight load bearing applications [1]. Their corrosion and chemical resistance further enable use in demanding environments, including fluid-transport pipelines and storage vessels. Industrial adoption has grown rapidly in the past decade, driven by the need for durable, high-performance, and lightweight components.

A variety of manufacturing techniques are employed to produce tubular composites, ranging from manual fabrication to highly automated processes [2-5]. Established methods such as filament winding, Automated Fiber Placement (AFP), and Pull winding provide different benefits in terms of fiber control, production speed, and geometric versatility. Despite this progress, key challenges persist, including maintaining consistent part quality (e.g., minimizing voids and fiber misalignment), reducing overall manufacturing costs, and mitigating the environmental impact of composite fabrication and disposal.

To address these manufacturing challenges, new process concepts are being developed to enhance efficiency, quality, and sustainability. Among them is OLLOW's tape-winding approach [6], which draws inspiration from filament winding and automated fiber placement. In this method, unidirectional thermoplastic tapes are helically deposited onto a solid mandrel at prescribed angles without immediate matrix consolidation. The process is illustrated in Figure 1. Local weld points at the preform ends provide sufficient stability for handling. After winding, the preform is removed from the mandrel and transferred into a rigid metallic mold, where high pressure using an internal silicone membrane, and temperature are applied to produce the final straight or curved tube (Figure 2).

This decoupled winding/consolidation workflow offers notable advantages over traditional techniques. Automated tape winding improves repeatability and dimensional accuracy, while separating consolidation from deposition shortens production cycles and supports high-throughput

manufacturing. The reliance on thermoplastic matrices further decreases cycle times [7] and enables recyclability, reducing the overall environmental impact. As a result, this process shows strong promise for scalable, cost-efficient, and sustainable production of tubular composite structures across diverse industrial sectors.

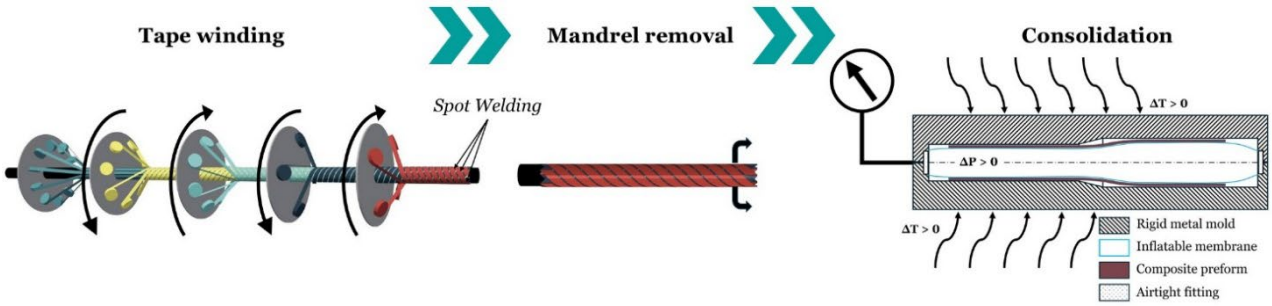

Fig. 1. The manufacturing process involves two main stages: dry winding onto the mandrel and thermoforming inside a rigid die, using heat and pressure.

Fig. 2. A bicycle handlebar constructed from several consolidated tubes, each featuring a different cross-sectional shape

Although the technology offers clear advantages, it is not without challenges. A key issue examined in this study is the loss of dimensional stability that occurs when the preform is removed from the mandrel. Certain layup configurations, particularly specific combinations of winding angles, exhibit pronounced instability upon release: the preforms undergo significant axial expansion and radial contraction, triggering a rapid geometric collapse. This sudden deformation forces the individual tapes to reorganize, disrupting the intended fiber orientations and compromising the mechanical properties of the final part. In severe cases, as illustrated in Figure 3, the preforms become unusable and must be discarded. While industrial mitigation strategies exist, they typically require adding extra tape layers to stabilize the layup, which increases cycle time, defect risk, and final component weight. A deeper understanding of the instability mechanisms of helically wound tapes is therefore essential for reducing scrap and improving overall manufacturing efficiency.

Fig.3. Upon removal from the mandrel, some preforms undergo significant axial expansion and a reduction in their inner diameter

Helical stability of slender structures has been investigated in the literature. It has been demonstrated that certain helical configurations of elastic rods remain stable only when their length is sufficiently short, typically for helices comprising less than one full revolution [8-10]. Borum et al. [11] analyzed the stability of helical equilibria of inextensible, isotropic Kirchhoff rods clamped at both ends, employing the conjugate point method to determine the maximum stable length of a helical equilibrium. The stability of strips/rods with asymmetric cross sections has also been addressed in previous studies. Goriely et al. [12] showed that only configurations without intrinsic twist, with the principal bending direction aligned with either the normal ($\overline{fr_2}$ in figure 2) or binormal vector ($\overline{fr_3}$ in

figure 2) of the local Frenet frame, can form helical equilibria from an initially straight state. In this context, wound ribbons can be interpreted as binormal strips. According to Goriely et al. [13], infinitely long binormal strips bent into a helical configuration are inherently unstable, whereas finite-length strips can attain stability if their cross-section is sufficiently flat, that is, if the thickness to width ratio is small. Additional studies have explored instability in helically deformed structures arising from mechanical anisotropy, where geometric or material parameters govern spontaneous shape transitions [14-15]. The stiffness of helices under tension has also been quantified: Starostin et al. [16] derived an expression for the equivalent spring stiffness as a function of helix angle and cross-sectional properties, later validated experimentally by Prévost et al. [17]. These findings collectively indicate that helix stiffness decreases with unwinding length, helix angle, and torsional-to-bending stiffness ratio.

Despite these advances, the stability of helically wound ribbons composed of anisotropic materials remains largely unexplored. The mechanical response of such ribbons upon release of winding constraints is, to date, insufficiently studied.

This study examines how wound tapes reorganize during preform release, focusing first on the displacement of individual tapes under varying properties. An experimental setup is developed to replicate mandrel removal, and its results are used to validate a numerical model. The work also introduces the concept of layer equivalent stiffness to clarify how multi-layer behavior emerges and concludes with simulations of full multi-layer preforms to assess their global stability during release.

Stability of the Individual Composite Tape

Before qualifying the instability problem on the scale of the preform, the phenomenon is studied at the scale of an individual carbon fiber reinforced polymer (CFRP) tape. Numerical as well as experimental procedures are designed in this work to reproduce this behavior. An original experimental setup was built and used to simulate the winding and releasing of the tapes. Its results were then compared to numerical ones using the Finite element (FE) software ABAQUS. The stress state and deformation mechanisms were also evaluated using the numerical model, which was later used to conduct a parametric study of the tape geometric and mechanical properties.

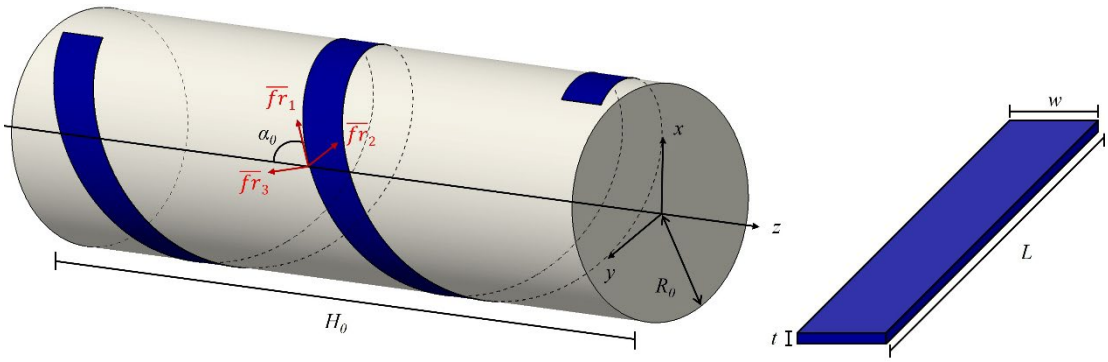

Fig. 4. An individual tape wound onto a mandrel, along with the corresponding geometric properties

The considered geometric properties of the tapes are the following: tape winding angle α, winding radius R, tape width w, tape thickness t, tape unwound length L, number of revolutions N_{rev}, and tape wound height H. The parameters α, R, and H will evolve once the mandrel is released. For this reason, quantities referring to the as-wound configuration (prior to mandrel removal) are denoted with a subscript 0. The initial winding angle α_0 (cf. Figure 4) is defined as the angle between the tape's tangent vector (expressed in the conventional Frenet frame of the helix shown in the figure) and the mandrel axis. Consequently, $\alpha_0 = 0°$ corresponds to a tape laid flat and parallel to the mandrel axis, whereas $\alpha_0 = 90°$ corresponds to a tape wound into a closed ring. These parameters are related through the helix geometry given in Eq. 1, which hold for any regular helix.

$$\begin{cases} L = 2\pi N_{rev} R_0 \dfrac{1}{\sin(\alpha_0)} \\ H_0 = \dfrac{2\pi N_{rev} R_0}{\tan \alpha_0} \end{cases} \quad (1)$$

Experimental procedure. The experimental setup presented in Figure 5 was specifically designed to simulate the releasing phase of the preforms from the mandrel. It consists of two plastic wire supports through which nylon wires are threaded. The wires are fixed to one support (the left support in Figure 5) and tensioned at the opposite end using a wire-tensioning mechanism. This mechanism includes a disc to which the wires are bolted; the disc is actuated by a pulley system to apply tension. Under tension, the wires form a quasi-mandrel onto which the tapes are wound. The design of both the wire supports and the tensioning system enables the creation of a fully collapsible mandrel.

Each support contains a set of evenly spaced holes along the perimeter of a circle corresponding to the desired winding radius. When the wires are tensioned, they assume this circular geometry, whereas releasing the tension causes the mandrel to collapse entirely. The winding radius used in all experiments is 20 mm.

The tape is secured in the wound configuration at two fixation regions. At segment A, the tape is rigidly clamped using a bolted fixture, constraining all degrees of freedom (DoF). At segment B, the tape is mounted on a linear slide and fixed with bolts such that only axial translation along the mandrel direction (the z-axis) is permitted. After winding, the wire tensioning system is released, allowing the mandrel to collapse and enabling the tape to translate along the linear slide. Depending on the winding angle and tape geometry, this results in either an increase or a decrease in the tape height.

The test is performed 3 times and the elongation of the ribbon ΔH is then averaged. Finally, the relative elongation $\Delta H/H_0$ is then reported for each winding angle.

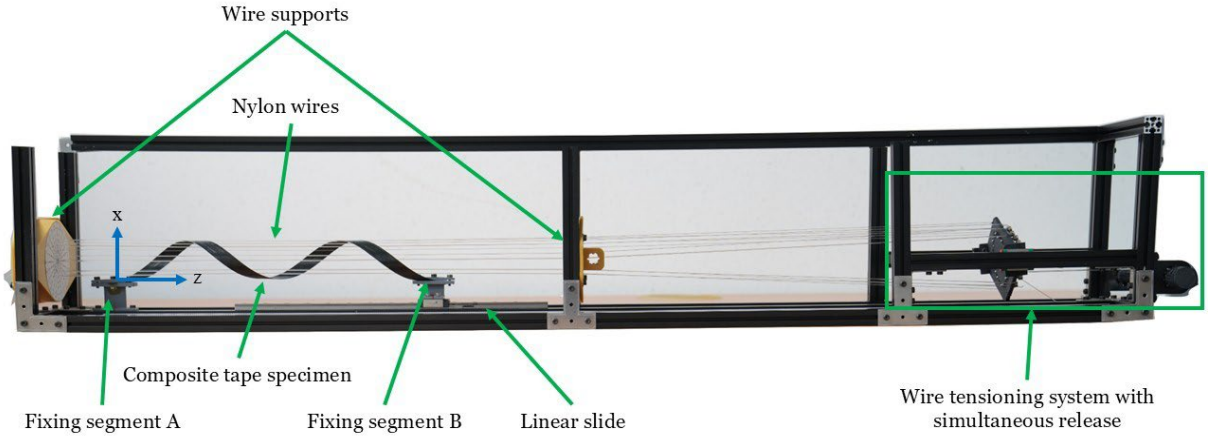

Fig.5. Experimental setup for releasing individual wound tapes

Carbon fiber reinforced thermoplastic tapes with a polyamide-6 matrix (CF-PA6) are investigated in this study. They are referenced to as CF6 tapes in this work. The transversely isotropic elastic properties and cross-sectional geometrical characteristics of the tapes are summarized in Table 1, where V_f denotes the fiber volume fraction. The mechanical properties of the constituent fibers and matrix were obtained from literature sources [18,19] and from manufacturers' datasheets. These properties were subsequently used to derive the effective transversely isotropic properties of the unidirectional tapes using classical rule of mixtures formulations, which provide an adequate representation for unidirectional composite laminates [18].

Experimental tests were conducted for initial winding angles α_0 ranging from 20° to 70° with a single revolution (N_{rev} =1). Smaller winding angles could not be investigated for larger values of N_{rev} due to geometric limitations of the experimental setup. Moreover, for increasing α_0, a higher number of revolutions significantly amplifies ribbon instability, rendering the post-release response highly

sensitive to experimental conditions such as release rate, ambient vibrations, and small variations in the initial angle. As previously reported in [11,12], helically wound structures exhibit pronounced instability as their length increases. Consequently, instability becomes a limiting factor for experiments involving large N_{rev}. To mitigate these effects, the mandrel was released quasi-statically during the experiments to promote the formation of the elongated ribbon configuration. Rapid release of the wire-tensioning system was found to introduce vibrations that strongly affect the response in highly unstable configurations. Gradual release of the applied tension effectively suppresses these unwanted vibratory effects.

Tape specimens were cut to the exact required length using the geometric relations given in Eq. 1. Prior to winding, the samples were kept straight under applied weights to ensure an initially straight configuration. The tapes were then mounted onto the experimental setup by bolting their extremities at fixing segments A and B. The initial winding angles were measured using a protractor in these fixing regions. Before mandrel release, the wound height H_0 and mandrel radius R_0 were also measured to verify the accuracy of the prescribed initial winding angle.

Numerical model. A finite element model is developed using the commercial software ABAQUS to simulate the mechanical response of individual composite tapes. The numerical results are subsequently compared with the corresponding experimental observations.
A dedicated pre-processing stage is implemented using a Python script to generate the spatial trajectories of the tape nodes and to construct the finite element mesh. Based on this information, an ABAQUS input file is automatically generated, containing all geometric, material, and boundary-condition data required for the simulations.
The analysis is performed using two quasi-static steps with geometric nonlinearity enabled to account for large displacements and rotations. Both steps are solved using an implicit time-integration scheme. In the first step, the initially straight, stress-free tape is clamped at one extremity, corresponding to segment A in the experimental setup, while prescribed displacement boundary conditions, computed by the Python pre-processing code, are applied to impose the wound configuration. This winding step is illustrated in Figure 6.

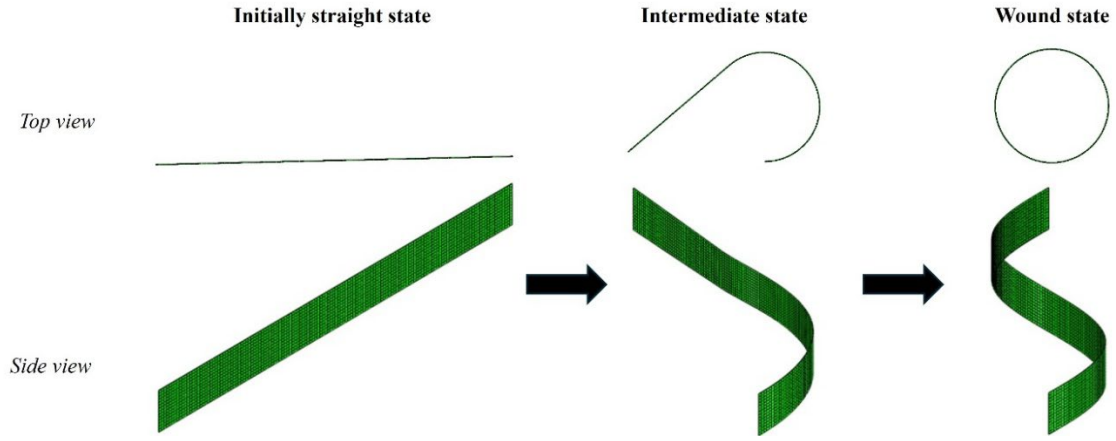

Fig. 6. The tapes are helically wound in the first step using displacement control of each node

In the second step, the prescribed displacement boundary conditions are removed to simulate mandrel release. The node set at the left extremity of the tape (segment A) is constrained in all DoFs. The right extremity of the tape (segment B) is then constrained in all DoFs except for translation along the mandrel axis (the z-direction), reproducing the experimental boundary conditions during release. The boundary conditions on the tape after completion of the winding step are chosen in accordance to the experimental ones. The tapes are meshed using quadrilateral shell elements. The mesh is constructed such that all element edges have equal length, ensuring uniform discretization. The number of elements across the tape width, denoted $N_{elements/width}$, is selected as the primary meshing parameter. A mesh convergence study is therefore performed to determine an appropriate discretization level. Convergence with sufficient accuracy is achieved for $N_{elements/width} = 14$, which is retained for the

remainder of the study as a compromise between numerical accuracy and computational cost. Linear elastic law with lamina anisotropic material section is created for transversely isotropic materials. The material properties used are taken from table 1 for model validation and for further parametric analysis.

Table 1. Tape geometric and mechanical properties

Material	t [mm]	w [mm]	V_f [%]	E_1 [GPa]	E_2 [GPa]	ν_{12} [-]	G_{12} [GPa]	G_{23} [GPa]
CF-PA6	0.15	12.7	48	110	4.19	0.29	1.54	1.53

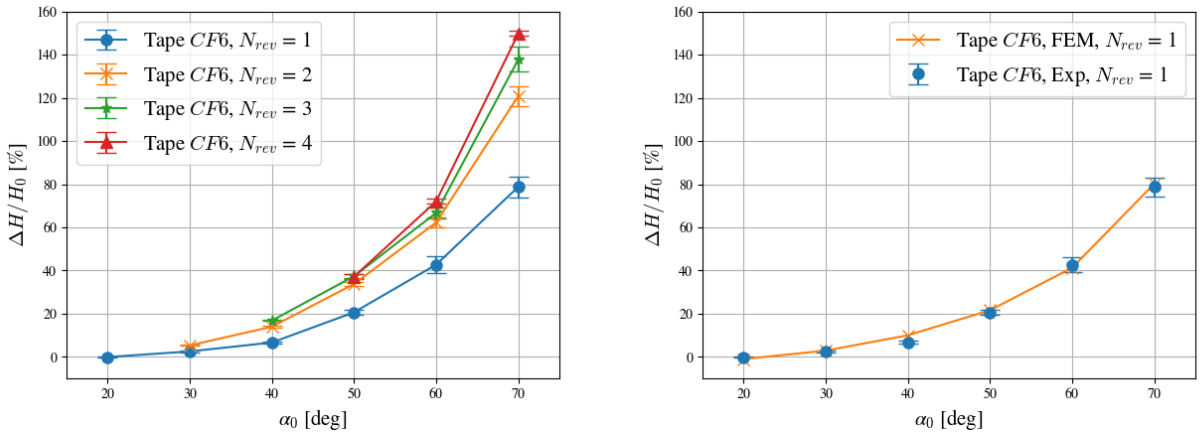

Fig. 7. Experimental (left) and numerical results validation (right) of the CF6 tape

Results Figure 7 shows the results of releasing of the tape CF6. As shown in Figure 7 (left), the reported experimental results predominantly exhibit a positive relative elongation following mandrel release. Small negative elongation is observed only in a limited number of cases, primarily for small initial winding angle α_0 = 20°, where measured elongation reaches -0.04%. A pronounced increase in the elongation response is observed with increasing α_0 indicating a strong dependence of the post-release deformation on the initial winding angle. In addition, increasing the number of revolutions N_{rev} leads to a larger elongation response, manifested by higher curves. The response also becomes progressively smoother and less affected by experimental noise as N_{rev} increases.

Because both extremities of the ribbon are rotationally clamped, the achievable elongation is constrained by boundary effects. However, increasing the number of revolutions introduces a larger central region of the helix that is less influenced by these constraints and can deform more freely. Consequently, the influence of the boundary conditions is progressively reduced as N_{rev} increases. To validate the numerical model, finite element (FE) results are compared with experimental measurements for the case N_{rev} =1, which remains numerically stable across all investigated winding angles.

The numerical and experimental results are plotted together in Figure 7 (right). A good agreement is observed between the FE predictions and experimental measurements of relative elongation, both qualitatively and quantitatively, supporting the validity of the proposed numerical model.

Upon release from the mandrel, the ribbon evolves toward a configuration that minimizes its internal strain energy. Under the imposed boundary conditions, this relaxation occurs through changes in the helix height H, radius R, and winding angle α, which are the only geometric parameters free to evolve.

Effect of geometric and mechanical properties of the tape. The study has concluded the following after a parametric study of the tape mechanical and geometric properties:

- The initial winding angle α_0 has a strong influence on the mechanical response of the ribbons. For the composite tape considered in this study, the response becomes increasingly sharp as α_0 increases. The relative elongation–winding angle curves exhibit a pronounced nonlinear behavior. In particular, for larger winding angles, the composite tapes undergo significantly higher elongation.

- The cross-sectional geometry of the tape significantly influences its mechanical response. An increase in tape width is found to reduce the relative elongation, particularly at larger winding angles. In contrast, variations in tape thickness within the investigated range do not produce a noticeable effect on the elongation response.
- The winding radius has a positive influence on the elongation response of the composite tapes, particularly at larger winding angles. Analysis of the post-release angular profiles for tapes with different initial winding radii indicates the presence of a preferred equilibrium angle in the high angle regime. The equilibrium angle depends on the mechanical and geometric properties of the tape, and is typically in the range of 20° to 30°. Reaching this equilibrium configuration requires larger axial elongation than that of smaller radii, which explains the increased elongation observed for larger winding radii.
- The influence of the mechanical properties in the longitudinal and transverse directions was investigated through a parametric variation of the material constants. In the longitudinal direction, an increase in the Young's modulus E_1 enhances the bending stiffness of the tape, thereby amplifying the elongation response. Conversely, increasing the transverse modulus E_2 has a mitigating effect on the response.
- The in-plane shear modulus G_{12} is found to significantly limit the elongation for larger initial winding angles α_0. Since G_{12} directly contributes to the torsional stiffness of the tape, increasing its value enhances the resistance to reductions in the helix angle during release, a deformation mode associated with higher torsional strains. Consequently, larger values of G_{12} suppress the elongation response in the high angle regime.

Layer Equivalent Stiffness

According to the results observed experimentally and obtained numerically, the wound strips behave like a loaded spring, either in tension or compression. When the mandrel is released, these springs return to their length at equilibrium. It would be interesting to evaluate the equivalent stiffness of these springs k_{eq}, which would allow us to predict the behavior of a preform when several tapes coexist. At first approximation, it can be assumed that the multi-tape preform consists of several springs in parallel, with different stiffnesses and equilibrium lengths. Starostin et al. [16] derived an analytical expression for the equivalent axial stiffness of a helical spring, expressed as a function of the helix angle as well as the cross-sectional geometric and mechanical properties. Their formulation accounts for the coupling between torsional and bending deformations inherent to helical geometries, thereby providing a comprehensive description of the global mechanical response under axial loading. Subsequently, Prévost et al. [17] experimentally validated this theoretical model, confirming its predictive capability across a range of geometrical configurations. The combined theoretical and experimental results demonstrated that the effective stiffness of a helical coil systematically decreases with increasing unwound length, increasing helix angle (winding angle), and with reductions in both torsional and bending stiffnesses of the constituent material. In the context of the present work, this framework is adapted to describe the stiffness of helically wound ribbons, wherein similar geometric and mechanical dependencies govern the effective stiffness response. The corresponding expression, tailored to the assumptions and boundary conditions of the current study, is presented in Eq. 2.

$$k_{ribbon} = \left[2\pi N_{rev} R_0^3 \sin^2(\alpha_0)\left(\frac{1}{C}\sin^2(\alpha_0) + \frac{1}{B}\cos^2(\alpha_0)\right)\right]^{-1} \quad (2)$$

where B and C represent the bending and torsional stiffness, respectively. The equivalent spring stiffness k_{ribbon} relates the force that the ribbon exerts in its extremities in its wound state, to the displacement in the axial direction when the winding boundary conditions are released. This expression reveals that the equivalent stiffness of the strips decreases as α_0 increases. Consequently, using smaller angles in the preform results in a 'stiffer' tape that stretches relatively less. In order to compare this expression to our case, a study was conducted using the FE model. After winding, a reference point in kinematically tied to the fixing segment B. The axial reaction force of the Reference

Point (RP) at the end of the ribbon RF_3 is measured in the as wound state. It represents the force that the ribbon exerts in the axial direction when wound.

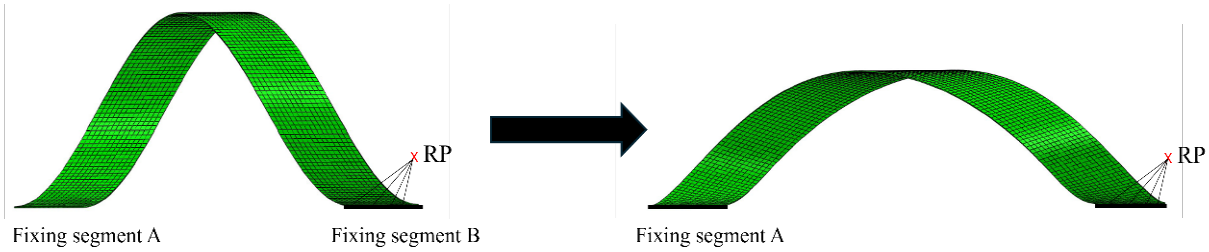

After Winding
- Clamp end segments
- Measure reaction force of RP (RF_3)

Last step
- Allow axial translation of segment B
- Measure displacement of RP (U_3)

Fig.8. Method for calculating the equivalent wound tape stiffness

The displacement U_3 of the same RP is measured after release of the winding boundary conditions. The equivalent stiffness k_{FE} is calculated using the following formula:

$$k_{FE} = \frac{RF_3}{U_3} \tag{3}$$

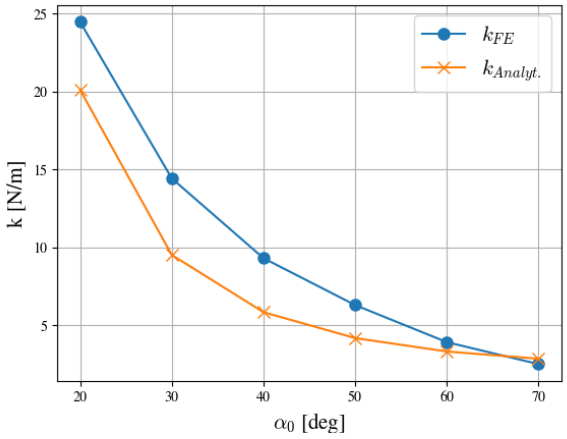

Fig. 9. Evolution of the equivalent stiffness of wound strips: comparison of the analytical and numerical models.

Figure 9 shows a comparison of the analytical stiffnesses calculated by [16] and [17] and that calculated by the finite element model. We can see the same non-linear decreasing trend in stiffness with the winding angle. This clearly shows that the larger angles that elongate the most have the lowest stiffness. On a complete preform, smaller angles that elongate less and have greater stiffness would need to be combined to prevent or limit this elongation.

Stability of Preforms

After studying the stability of ribbons on a simple scale, more complex cases can be examined. Preforms consisting of several ribbons can be simulated using the same finite element model described above, in order to analyze the influence of combining different winding angles. In this study, a preform consisting of two layers of five ribbons is simulated. The initial height of the preforms H_0 is set at 300 mm. The objective is to observe the interaction between layers with different winding angles. The ribbons used to manufacture the preforms have the same properties as those given in Table 1. After the winding step, surface-to-surface contact is activated between the two layers of the preform, and the layers are welded together at their ends using rigid connectors. The purpose of this welding is to connect all the ribbons in such a way as to prevent excessive isolated displacement of an individual ribbon, which could lead to numerical instability and divergence of the

analysis. The winding orientation is alternated for each layer (right-hand helices in the first layer and left-hand helices in the second layer), and the ribbons are positioned to minimize gaps in the preform. The smallest angles are always placed in the inner layer.

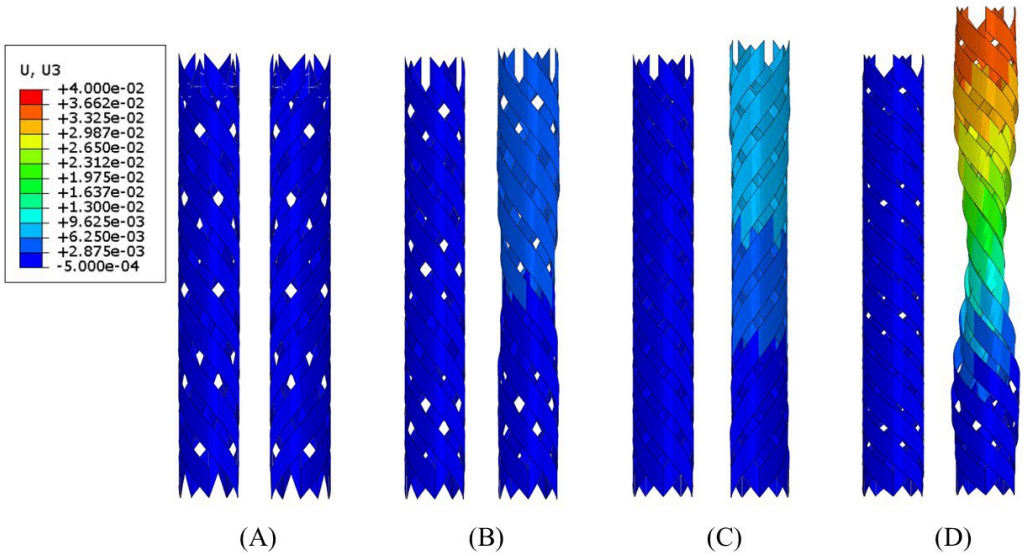

Fig. 10. Overview of the simulated preforms: The layups are laid in pairs of as-wound (left) and released (right). From left to right the preforms are.
Preform A : [5 × 20◦,5 × −40◦] ΔH = -0.2 mm, Preform B : [5 × 30◦,5 × −40◦] ΔH = 5.7 mm, Preform C : [5 × 40◦, 5 × −40◦] ΔH = 9.5 mm, Preform D : [5 × 40◦,5 × −50◦] ΔH = 34.0 mm

The reference preform studied has winding angles of 40° in the inner layer and -40° in the outer layer. Other preform configurations are compared to this one. The following layups are simulated: [5 x 20°, 5 x -40°], [5 x 30°, 5 x -40°], [5 x 40°, 5 x -40°] and [5 x 40°, 5 x 50°]. The results are presented in Figure 10, where each wound preform is illustrated alongside its deformed configuration after removal of the imposed displacements. As expected, the preform with the most dimensional stability is the first one, consisting of tapes at 20°(ΔH = -0.2 mm). As shown previously, small winding angles result in the lowest elongation values. As shown in Figure 10, axial expansion occurs gradually for increasingly higher angles. The phenomenon of preform collapse is evident for the last preform on the right, which has the highest pitch angle (ΔH = 34 mm). Compared to the reference preform, the combination of 20° strips limits expansion by up to 99%. By combining different angles, the structural behavior of the preform can be compared to that of a parallel spring system. By examining the equivalent spring stiffness of each wound ribbon, the final expansion of the preform can be estimated. This proves that combining lower angles with higher ones would limit the instability greatly.

Conclusion

In this work, the post-release behavior of helically wound ribbons was examined through a combined experimental and finite element (FE) approach. The FE model was validated against the experimental measurements and subsequently employed to identify the principal factors governing the axial response of the structure. The results demonstrate that both the mechanical properties and the cross-sectional geometry of the ribbon play a critical role in determining the axial displacement that develops following mandrel removal. An equivalent spring stiffness associated with a wound ribbon was derived, providing a first order approximation of the instability of a multi-layer preform, modeled as a system of parallel springs with distinct stiffnesses and rest lengths. The validated FE model was further used to simulate the behavior at the scale of complete preforms, revealing the interactions between layers wound at different angles. These simulations confirm that the inclusion of layers with smaller winding angles contributes to an overall increase in the stability of the layup.

Future research should address multi-layer preforms, as combining tapes of different materials or cross-sectional shapes offers a potential strategy for controlling structural instability. The influence of inter-layer friction should also be considered, as frictional interactions may restrict relative sliding between layers and thus affect the collapse behavior. Additionally, tailored welding strategies, such as welding unstable layers to more stable ones, could further enhance the dimensional stability of the final preform.

References

[1] S.M. Kennedy, R.J. Robert, R.M.R. Prince, G. Hikku and M. Kaliraj, "A comprehensive overview of the fabrication and testing methods of frp composite pipes," MethodsX, vol. 13, p.102990, 2024.

[2] J. Singh, K. Singh, J. S. Saini, and Mohammed S.J. Hashmi, "Processing of Polymers and Their Composites: A Review," Elsevier eBooks, pp. 577–603, Jan. 2018.

[3] M. Azeem, H. H. Ya, M. A. Alam, M. Kumar, P. Stabla, M. Smolnicki, L. Gemi, R. Khan, T. Ahmed, Q. Ma et al., "Application of filament winding technology in composite pressure vessels and challenges: a review," Journal of Energy Storage, vol. 49, p. 103468, 2022.

[4] A. Brasington, C. Sacco, J. Halbritter, R. Wehbe, and R. Harik, "Automated fiber placement: a review of history, current technologies, and future paths forward," Composites Part C: Open Access, vol. 6, p. 100182, 2021.

[5] M. Volk, O. Yuksel, I. Baran, J. H. Hattel, J. Spangenberg, and M. Sandberg, "Cost-efficient, automated, and sustainable composite profile manufacture: A review of the state of the art, innovations, and future of pultrusion technologies," Composites Part B: Engineering, vol. 246, p. 110135, 2022.

[6] B. Laine and A. Azran, "Device for the manufacturing of an unconsolidated textile elongate member." Patent WO 2023/089 051 A1, WO 2023/089051 A1. May, 2023.

[7] M. Kropka, M. Muehlbacher, T. Neumeyer, and V. Altstaedt, "From ud-tape to final part–a comprehensive approach towards thermoplastic composites," Procedia CIRP, vol. 66, pp. 96–100, 2017.

[8] N. Chouaieb, A. Goriely, and J. H. Maddocks, "Helices," Proceedings of the National Academy of Sciences, vol. 103, no. 25, pp. 9398–9403, 2006.

[9] A. Majumdar and A. Raisch, "Stability of twisted rods, helices and buckling solutions in three dimensions," Nonlinearity, vol. 27, no. 12, p. 2841, 2014.

[10] A. Goriely and M. Tabor, "The nonlinear dynamics of filaments," Nonlinear Dynamics, vol. 21,pp. 101–133, 2000.

[11] A. Borum and T. Bretl, "When is a helix stable?" Physical review letters, vol. 125, no. 8, p. 088001, 2020.

[12] A. Goriely, M. Nizette, and M. Tabor, "On the dynamics of elastic strips," Journal of Nonlinear Science, vol. 11, pp. 3–45, 2001.

[13] A. Goriely and P. Shipman, "Dynamics of helical strips," Physical Review E, vol. 61, no. 4, p. 4508, 2000.

[14] Q. Guo, A. K. Mehta, M. A. Grover, W. Chen, D. G. Lynn, and Z. Chen, "Shape selection and multi-stability in helical ribbons," Applied Physics Letters, vol. 104, no. 21, 2014.

[15] Z. Chen, "Shape transition and multi-stability of helical ribbons: a finite element method study,"Archive of Applied Mechanics, vol. 85, pp. 331–338, 2015.

[16] E. Starostin and G. Van Der Heijden, “Tension-induced multistability in inextensible helical ribbons,” Physical review letters, vol. 101, no. 8, p. 084301, 2008.

[17] L. Prévost, A. Lindner, and O. Du Roure, “Pitch controls the flexibility of helical ribbons,” Extreme Mechanics Letters, vol. 58, p. 101923, 2023.

[18] L. N. McCartney, “Predicting properties of undamaged and damaged carbon fibre reinforced composites,” in The Structural Integrity of Carbon Fiber Composites: Fifty Years of Progress and Achievement of the Science, Development, and Applications. Springer, 2016, pp. 425–467.

[19] E. Kurkin, M. Spirina, O. U. Espinosa Barcenas, and E. Kurkina, “Calibration of the pa6 short-fiber reinforced material model for 10% to 30% carbon mass fraction mechanical characteristic prediction,” Polymers, vol. 14, no. 9, p. 1781, 2022.